2013-11-26

Deformation coupling between the Archean Pukaskwa intrusive complex and the Hemlo shear zone, Superior Province, Canada

Liodas, NT

10.1016/j.tecto.2013.06.022
Tectonophysics

Tectonophysics 608 (2013) 1226–1237

Contents lists available at ScienceDirect

Tectonophysics

journal homepage: www.elsevier.com/locate/tecto

Deformation coupling between the Archean Pukaskwa intrusive complex and the Hemlo shear zone, Superior Province, Canada

Nathaniel T. Liodas [a], Aude Gébelin [b,c], Eric C. Ferré [a,*], Girmay M. Misgna [d]

[a] Department of Geology, Southern Illinois University, Carbondale, IL 62901, USA
[b] Biodiversity and Climate Research Centre (BiK-F), Senckenberganlage 25, 60325 Frankfurt/Main, Germany
[c] Department of Earth Sciences, University of Waterloo, Waterloo, Ontario N2L3G1, Canada
[d] Environmental Resources and Policy, Southern Illinois University, Carbondale, IL 62901, USA

ARTICLE INFO

Article history:
Received 19 February 2013
Received in revised form 12 June 2013
Accepted 20 June 2013
Available online 28 June 2013

Keywords:
Archean
Pukaskwa
Hemlo
TTG
Superior Province
AMS

ABSTRACT

Archean greenstone belts typically form narrow sheared basins separating bulbous tonalo–trondjhemo–granodioritic (TTG) intrusive complexes. The role played by gravity in the development of such dome-and-keel structures constitutes a key question in Archean tectonics. The Pukaskwa intrusive complex (PIC)–Hemlo greenstone belt system stands as a remarkable example of the dome-and-keel architecture that commonly occurs in Archean terrains. Abundant strain markers in the greenstone belt and in the Hemlo shear zone (HSZ) attest of late sinistral strike-slip kinematics (D_2) whereas, in general, the quartzofeldspathic coarse-grained rocks of the Pukaskwa intrusive complex bear little macroscopically visible kinematic indicators, most likely due to pervasive recrystallization. The PIC consists dominantly of a heterogeneous assemblage of TTG plutonic rocks and gneisses, which overall are less dense than the greenstone rocks. The study of anisotropy of magnetic susceptibility (AMS), based on 120 stations and 1947 specimens from the PIC, reveals east–west trending prolate and plano-linear fabrics across the northern margin of the complex, i.e., along the HSZ. Since geotherms were higher in the Archean than in the present, the effective viscosity of the TTG units would have been sufficiently low to allow their diapiric ascent through denser greenstone rocks. Here we propose an alternative model where thrust tectonics is responsible for the early structuration of the PIC. Later transpressive tectonics causes strain localization along internal strike-slip shear zones and along lithological boundaries.

1. Introduction

Density contrasts in a thin and hot lithosphere might have been the main force driving Archean orogenesis rather than plate tectonics (e.g., Chardon et al., 2009; Hamilton, 1998). Yet evidence for early plate tectonics makes this issue rather controversial (de Wit, 1998; Percival, 1994). The dynamic relationship between greenstone belts and tonalo–trondjhemo–granodioritic (TTG) complexes appears central in the "vertical tectonics" vs "horizontal tectonics" debate. The relatively low density of TTG complexes and associated anatectic gneisses might have allowed their diapiric rise through an overburden made of higher density mafic to ultramafic greenstone volcano-sedimentary rocks (Dixon and Summers, 1983). The geometry resulting from such process would resemble that of metamorphic core complexes (Lister and Davis, 1989). Alternatively, greenstone belts may have provided a buttress against which TTG complexes were emplaced. These two tectonic scenarios are not fundamentally incompatible and might have occurred simultaneously in the same region (Lin, 2005). Density-driven tectonics resulted in formation of large-scale dome-and-keel structures that characterize Archean terrains (Chardon et al., 1996; Harris et al., 2012; Lana et al., 2010; Lin, 2005; Sandiford et al., 2004; Shackleton, 1995; Van Kranendonk et al., 2010). Interference folding has also been proposed as a mechanism to explain structural domes within the Archean Chinamora batholith in Zimbabwe (Snowden and Bickle, 1976).

In order to advance our understanding of these important tectonic issues, we chose to study a representative example of a dome-and-keel structure in the Archean Superior Province, the Pukaskwa intrusive complex (PIC)–Hemlo shear zone (HSZ) system (Fig. 1). The Hemlo greenstone belt is part of the Wawa subprovince to the south of the Superior Province and is bounded to the south by the Pukaskwa granodiorite. A strong deformation can be defined along the northern margin of the granitic complex while moving away from the contact zone macroscopic structural markers become scarce. With the anisotropy of magnetic susceptibility study (AMS) being recognized as a powerful technique for quantifying strain in weakly deformed rocks, particularly in granitic, gneissic and migmatitic domains (Charles et al., 2009; Ferré et al., 2003, 2004; Gébelin et al., 2006; Hasalova et al., 2008; Kruckenberg et al., 2010, 2011; Polteau et al., 2008; Schulmann et al., 2009), we conducted a AMS study in the northern margin of the PIC to better understand its mechanism of emplacement and to investigate the role played by vertical and horizontal tectonics

* Corresponding author. Tel.: +1 6184537368; fax: +1 6184537393.
E-mail address: eferre@geo.siu.edu (E.C. Ferré).

0040-1951/$ – see front matter © 2013 Elsevier B.V. All rights reserved.
http://dx.doi.org/10.1016/j.tecto.2013.06.022

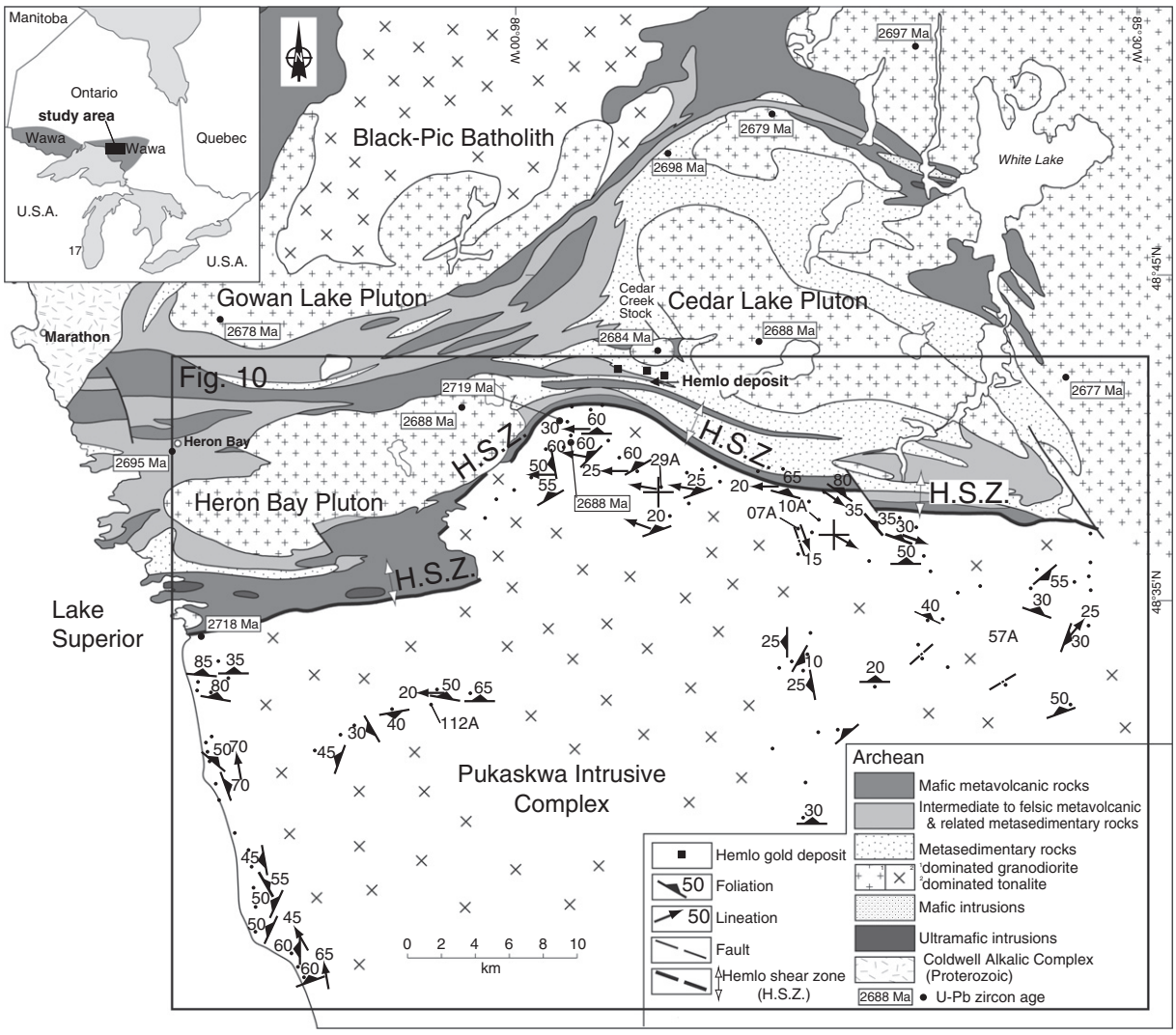

Fig. 1. Simplified geological map of the Hemlo greenstone belt modified after Lin (2001) showing the location of the Hemlo Shear Zone (H.S.Z.) and foliations and lineations measured in the northern margin of the Pukaskwa Granitic Complex (PIC). Small black dots indicate the locations of AMS data.

in Archean times. In these types of rocks, the AMS records the shape-preferred orientation of paramagnetic or ferromagnetic s.l. grains, which is generally acquired during plastic flow either at high- or low-temperatures. The AMS scalar parameters are calculated from the second rank tensor of magnetic susceptibility while the AMS vectorial parameters are given with respect to the geographic orientation of the specimen (Pokorny et al., 2004). The chosen example is not only representative of Archean processes but also relevant from an economic standpoint owing to the gold deposits hosted by the HSZ. The results of these investigations will advance our knowledge of Archean tectonics in the Superior Province, and potentially aid in the exploration of other prospective shear zones and intrusive complexes.

2. Regional setting

The Hemlo greenstone belt and the PIC are both located in the Wawa subprovince of the Superior Province in Ontario (Canada) (Fig. 1). The Superior Province forms the largest Archean terrain on Earth, covering an area of ≈1500 × 2500 km (e.g., Hamilton, 2007) and, like most Archean cratons, it originated from an amalgamation of different igneous and metamorphic terranes ranging in age between 3.10 and 2.65 Ga (e.g., Calvert and Ludden, 1999; Card, 1990). Geochronological data suggest that terrane assembly began with accretion of a magmatic arc (Card, 1990; Corfu and Muir, 1989a, 1989b; Percival et al., 2001; Williams et al., 1991).

2.1. Hemlo greenstone belt

The east–west striking Hemlo greenstone belt is bounded to the north and south by the two main large Black-Pic and Pukaskwa late Archean (~2720 Ma) tonalite–granodiorite granitoids (Beakhouse and Davis, 2005.), respectively. It is well known for containing one of the largest gold deposits in Canada localized along the HSZ (Fig. 1). The E–W trending HSZ affects over a ~2-km wide zone Archean supracrustal rocks of the greenstone belt as well as the northern margin of the PIC. The map pattern of the HSZ most likely results from the irregular contact between one of the intrusives in the PIC and the Hemlo greenstone belt rather than from post-shearing folding. The greenstone belt is composed of mylonitic Archean metasedimentary and felsic, intermediate and mafic metavolcanic rocks (e.g., Lin, 2001) which are intruded by late Archean (~2680 Ma; Beakhouse and Davis, 2005) granodiorite–quartz monzodiorite plutons (Fig. 1; Heron Bay, Gowan and Cedar Lake). The supracrustal rocks deposited from ≥2720 Ma to 2688 Ma (Corfu and Muir, 1989a, 1989b; Jackson, 1998) experienced three main ductile deformation events. The regional deformational fabric (D_1) is overprinted by a second and main regional event (D_2) that

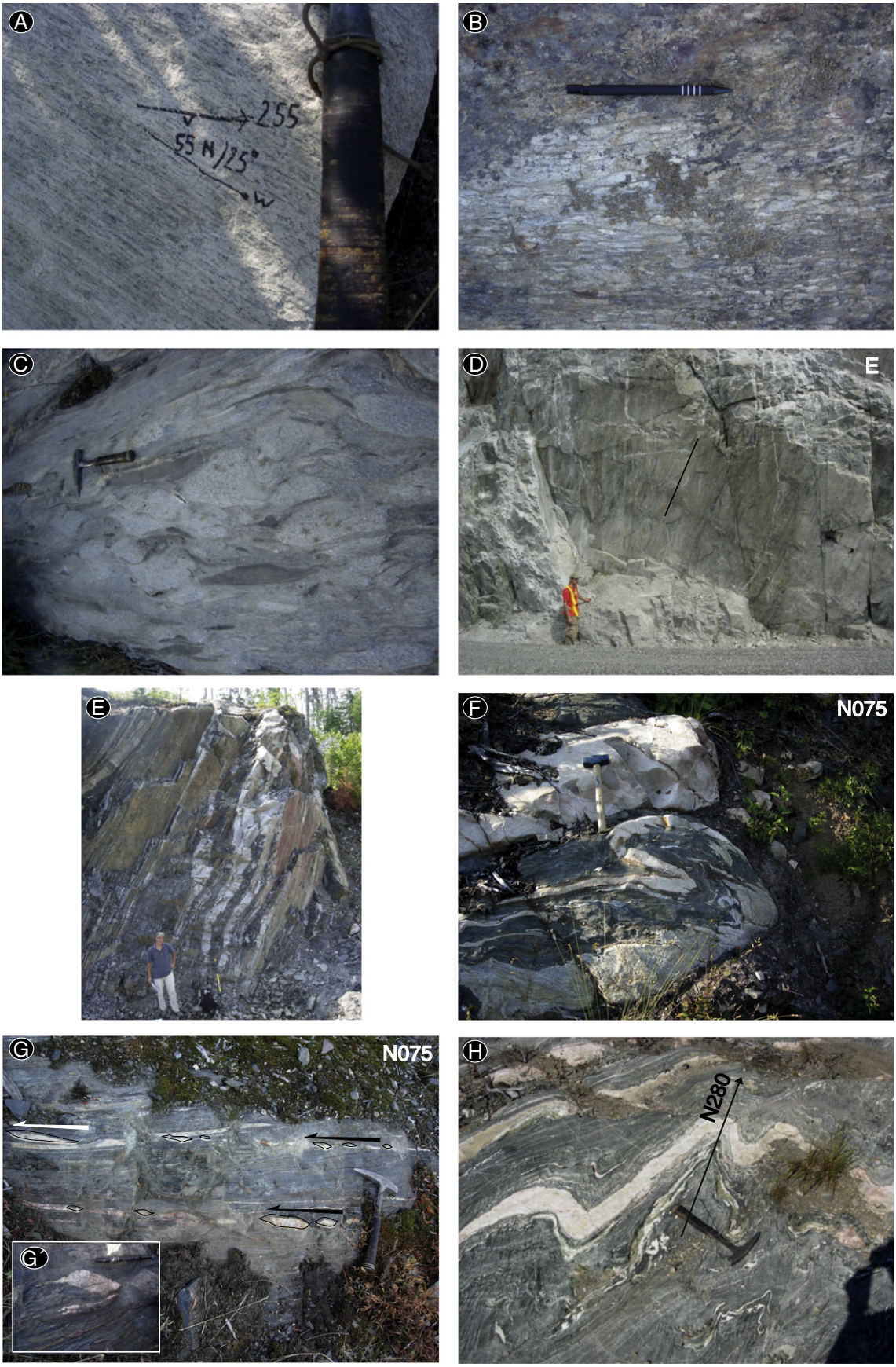
A
255
55 N/25°
W
B
C
D
E
E
F
N075
G
N075
G'
H
N280

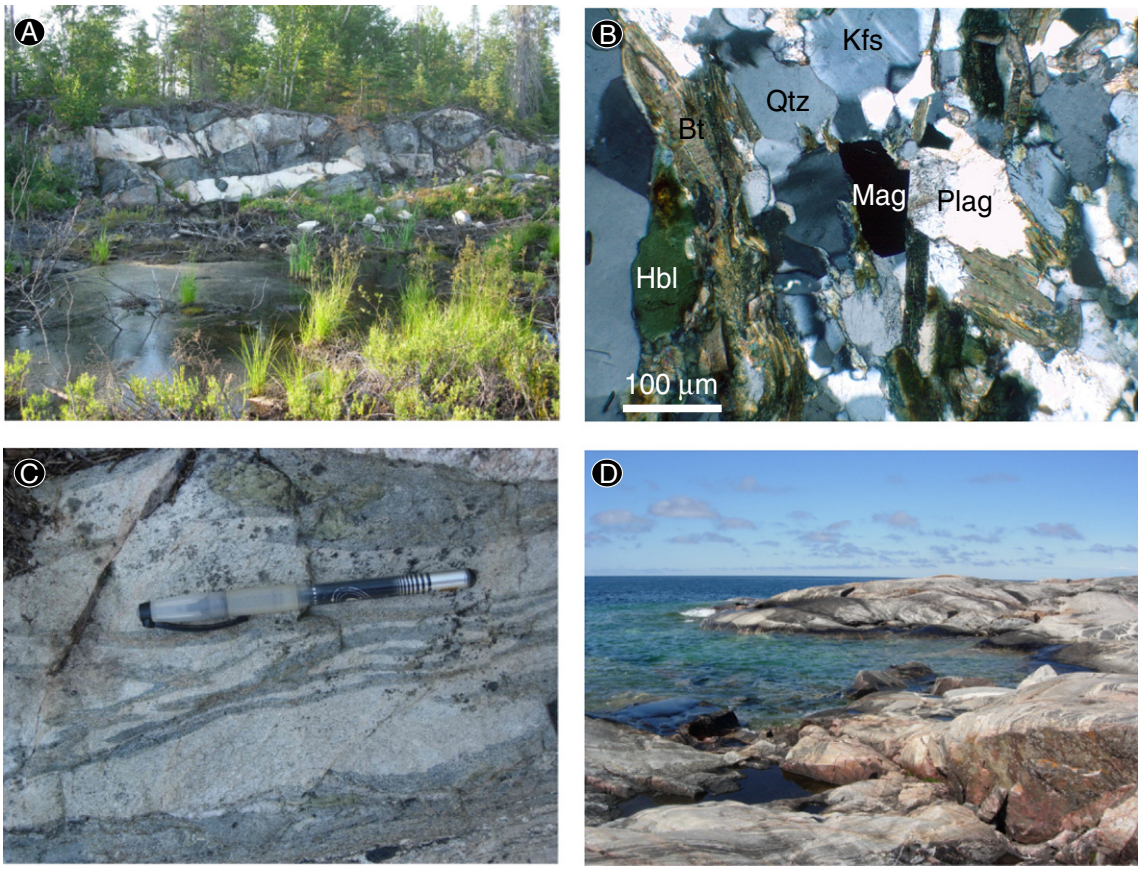

Fig. 3. Photographs of the Pukaskwa intrusive complex. (A) Amphibolite intruded by fine-grained leucocratic layers. Note the boudinage deforming the two rock types; (B) Biotite–hornblende–alkali feldspar–plagioclase–quartz–magnetite paragenesis observed on granodiorite to quartz monzodiorite rocks; (C) amphibolite facies metamorphic rocks experiencing partial melting. (D) Migmatite outcrop on the shoreline of Lake Superior (Oiseau Bay).

affects rocks within the HSZ. The foliation (S_2) dips steeply to the north (Fig. 1) and the lineation (L_2) defined by a preferred orientation of biotite and hornblende (Fig. 2A) and/or by elongate clasts in conglomerate (Fig. 2B) and/or volcaniclastic rocks (Fig. 2C) plunges steeply to the northwest in the shear zone center (Fig. 2D) to moderately move southward to the contact with the PIC (Fig. 2A). The foliation (S_2) is very well observed at the contact between the HSZ and the PIC where it is defined by compositional layering with layers rich in biotite and/or hornblende alternating with those rich in feldspar ± quartz (Fig. 2E). Associated folds F_2 are tight to isoclinal (Fig. 2F) and present a well-developed axial planar foliation (S_2). Kinematic criteria such as asymmetric folds (Fig. 2F) or boudins (Fig. 2G) indicate a top-to-the west sense of shearing. Based on the geometry of the main and possibly syn-D_2 ore deposit and observation of both cigar-shaped and pancake-shaped strain markers within the HSZ, Lin (2001) described it as a sinistral transpressional zone. A third event D_3, characterized by open to tight folds with a well-developed axial planar crenulation cleavage (Fig. 2H) is coeval with an oblique dextral shearing event (Lin, 2001). The peak metamorphism of amphibolite facies that characterized rocks of this region is dated at ~2677 Ma (Corfu and Muir, 1989a, 1989b), late or after D2 but before D3 (Lin, 2001).

2.2. Pukaskwa intrusive complex (PIC)

The PIC is bounded to the north by the Hemlo greenstone belt (Fig. 1) and to the south by the Mishibishu and Michipicoten greenstone belts. The lithologic diversity relates to the presence of pre-, syn-, and post-tectonic phases emplaced over an interval of 50 Ma from 2718 to 2667 Ma (Beakhouse and Davis, 2005; Beakhouse et al., 2011; Corfu and Muir, 1989a, 1989b). Five main lithologic units are distinguished based on their petrological and geochemical features: 1) mafic amphibolite (Fig. 3A); 2) foliated to gneissic tonalite to granodiorite (Fig. 2E); 3) granodiorite to quartz monzodiorite (Fig. 2A); 4) granite to granodiorite; and 5) pegmatite to aplite. The amphibolites of probable mafic metavolcanic origin are usually associated with granitic pegmatitic to aplitic dikes (Fig. 3A). The gneissic tonalites to granodiorites are thought to represent the pre-tectonic phases and derive from partial melting of basaltic crust at lower crustal or upper mantle depths. The granodiorite to quartz monzodiorite, which are more Mg-rich than the tonalite–granodiorite, but similar with respect to the high-Al, show evidences of increasing ultramafic components in their petrogenesis. Biotite and hornblende are the dominant minerals in equilibrium with titanomagnetite, alkali feldspar,

Fig. 2. Field photographs of the Hemlo shear zone. (A) Mineral lineation defined by biotite and hornblende plunging gently to the west (granodiorite to quartz monzodiorite, HSZ/PIC contact); (B) elongate clasts in conglomerate; (C) elongate clasts in volcaniclastic rocks; (D) Graywacke displaying northwesterly plunging down-dip lineation; (E) Near vertical layering of mafic (tonalite to granodiorite) and felsic layers at the contact between the HSZ and the PIC; (F) Asymmetric fold indicating a sinistral sense of shearing (amphibolitic and fine-grained leucocratic layers, HSZ/PIC); (G) and (G′) Asymmetric boudins displaying a-top-to-the west; (H) Third fold generation overprinting the S_2 foliation in amphibolitic and fine-grained leucocratic layers. Note the well-developed axial planar crenulation cleavage.

plagioclase and quartz (Fig. 3B). Granites and granodiorites represent the youngest phase and typically display a medium grained texture associated with a weak foliation. These granites and granodiorites most likely derive from partial melting of intermediate to felsic meta-igneous rocks. The lithological heterogeneities observed within the PIC must have caused significant rheological contrasts between rock types at high temperature leading to strain partitioning, particularly in areas around large amphibolite masses.

Most rocks show mineral assemblages typical of high-grade amphibolite facies metamorphic rocks (Fig. 3B) with abundant evidence of partial melting (Fig. 3C), giving rise to spectacular migmatites particularly well exposed on the shoreline of Lake Superior (Fig. 3D). Most outcrops exhibit a prominent and constant metamorphic foliation dipping steeply to the north at the contact with the greenstone belt that become variable away from it (Fig. 1). Mineral lineations trending ~E–W and plunging from 25° to 60° preferentially to the west in the northern margin are hardly definable within the granitic complex.

At the microscopic scale, a few areas display distinctively small grain size (5–50 μm). Quartz rarely displays undulose extinction and plagioclase does not exhibit mechanical twins. Plagioclase is commonly partially sericitized. Both hornblende and biotite form large subhedral, non-recrystallized grains (50–300 μm) that collectively mark a metamorphic foliation (Fig. 3B). Titanomagnetite forms stocky to prismatic, euhedral grains ranging in size from 5 to 200 μm. These elongated grains are free of exsolutions and are generally parallel to the long axis of mafic minerals (Fig. 3B).

Samples for AMS measurements were collected as most representative in volume and attitude of metamorphic/plutonic structure for the whole outcrop. This structural study excludes amphibolites, pegmatites and aplite dikes because these lithologic types represent less than 5% in volume of the main lithological phase. Due to limited accessibility in certain areas, sampling sites are heterogeneously distributed and concentrated on the northern margin of the PIC (Fig. 4).

3. Methods

3.1. Sampling procedure and sample preparation

A hundred and twenty oriented blocks (2–5 kg) were collected in the northwestern part of the PIC for AMS measurements. The scarcity of rock exposure in this heavily forested region constitutes a problem for sampling along a uniform grid. Oriented blocks were collected mostly along the lake shore, creeks and a few rare roadcuts. Samples were located using a portable global positioning system unit and oriented with respect to true north using a Brunton compass with accuracy better than 2°. At least two blocks were collected at each sampling locality. Each blocked yielded between 15 and 25 cubes. The samples were first reoriented and cut into 18.5 mm-thick horizontal

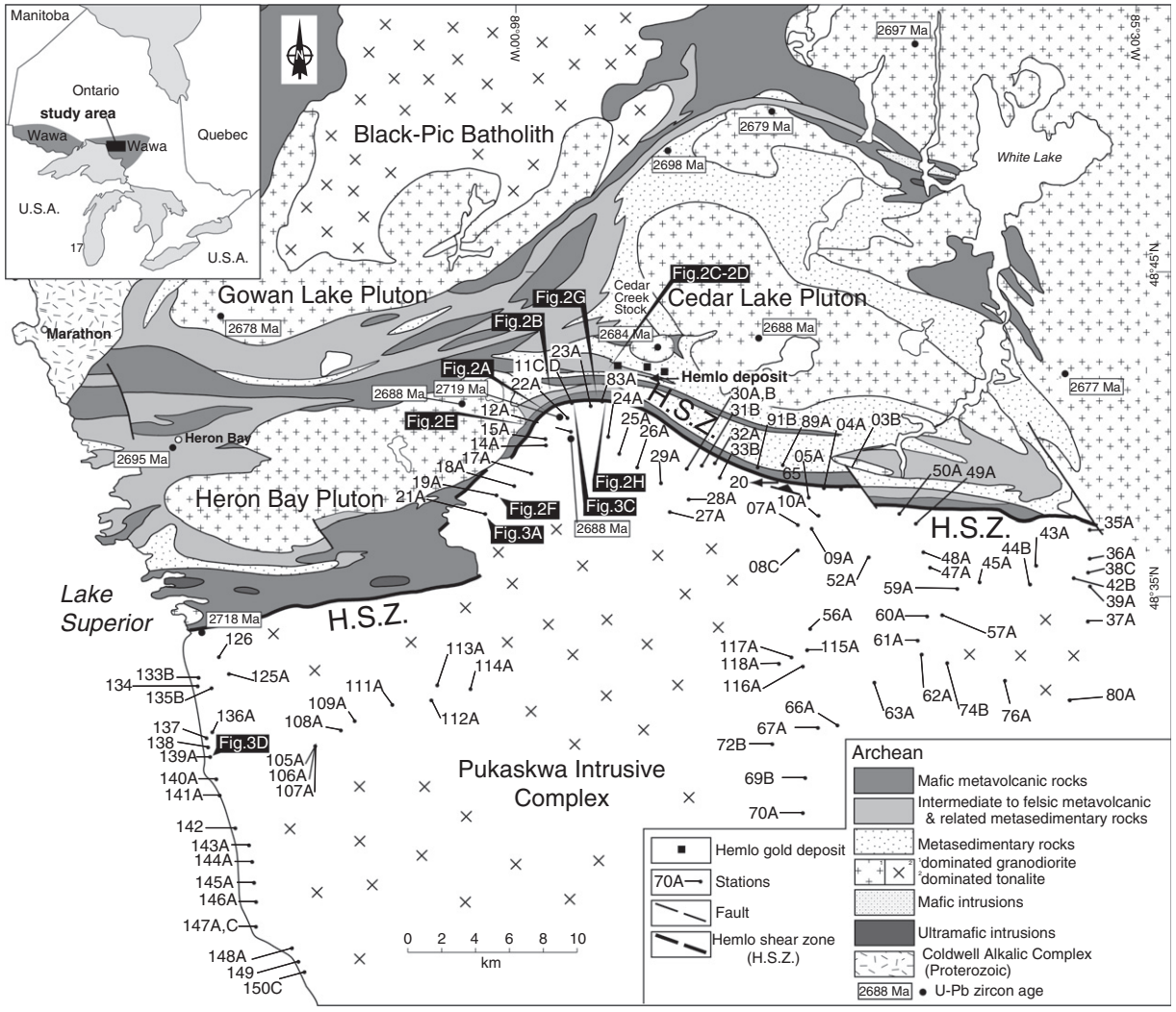

Fig. 4. Simplified geological map of the Hemlo greenstone belt modified after Lin (2001) showing the location of sampling sites and photographs seen in Figs. 2 and 3.

slabs, then cut into cubes. This process yielded 1947 oriented cubic specimens.

3.2. Measurements

AMS measurements were carried out on a *KLY-4S Kappabridge* magnetic susceptometer (Agico, Brno) under an alternating field of 300 A/m, 875 Hz. Each specimen was measured while slowly rotating about three mutually perpendicular axes (Pokorny et al., 2004). We provide the complete set of AMS data (AMS station averages of scalar and directional parameters) in Supplementary data 2; and AMS stereonets with confidence ellipses in Supplementary data 4. Thermomagnetic experiments (25–700 °C), under a field of 80 A/m and an operating frequency of 0.696 Hz, using a *Bartington MS2* furnace, provided the Curie temperature of the representative specimens. The magnetic hysteresis properties were measured on the same cubes as for AMS using a *Princeton Measurements Micromag 3900-04 vibrating sample magnetometer* with a sensitivity of $\approx 5 \cdot 10^{-9}$ Am^2, up to an applied direct field of 1.2×10^6 A/m. First Order Reversal Curve (FORC) data were processed using FORCinel (Harrison and Feinberg, 2008).

4. Results

4.1. Thermomagnetic experiment

Thermomagnetic experiments were performed in air on a representative crushed specimen up to 700 °C (Fig. 5) to determine the main carrier of magnetic susceptibility (K). This figure shows K normalized to K_0, the room-temperature low-field magnetic susceptibility, and expressed in percentage. The heating and cooling curves are broadly similar although the cooling curve attests to a slight gain in K. This phenomenon, common in plutonic rocks, results from additional magnetite formation from other mineral phases (Tarling and Hrouda, 1993). The magnetic susceptibility drops abruptly at 551 °C. This value, which is lower than the typical Curie temperature of pure magnetite (578 °C), indicates the presence of titanium in this titanomagnetite (Clark, 1997). We estimate the ulvöspinel content (x) in this titanomagnetite to 0.045, using the following empirical formula: T_c (°C) = 578 − 578x − 150x^2, where x is the ulvöspinel content (Clark, 1997). We interpret the distinct increase in magnetic susceptibility as the Hopkinson peak, a characteristic property of multi-domain magnetites (King and Ranganai, 2001). The increase in magnetic susceptibility observed between 600 and 700 °C is attributed to instrumental drift commonly observed on the Bartington furnace.

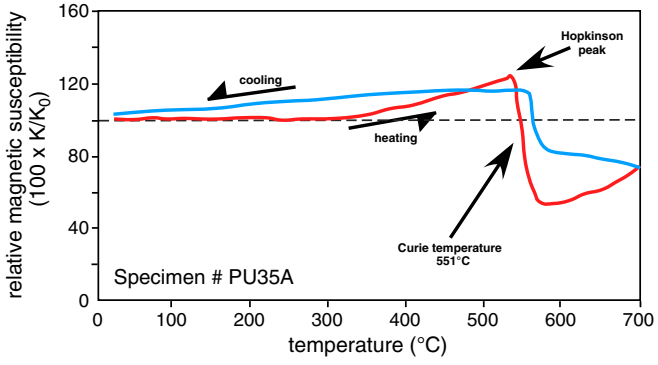

Fig. 5. Thermomagnetic experiment on a representative cubic sample. The variation of magnetic susceptibility as temperature increases is relatively constant up to ~350 °C. The increase in magnetic susceptibility before the Curie temperature is interpreted as the Hopkinson peak, which is characteristic of multi-domain magnetite (King and Ranganai, 2001). The Curie temperature (551 °C) is defined as the abrupt drop in magnetic susceptibility on the heating curve.

4.2. Magnetic hysteresis experiments and FORC analysis

We determined the magnetic hysteresis properties of 113 cubic specimens to evaluate magnetic domain grain size (Fig. 6). All specimens saturate magnetically below $16 \cdot 10^3$ A/m. The high-field magnetic susceptibility, K_{hf}, ranges from $3 \cdot 10^{-6}$ [SI] to $510 \cdot 10^{-6}$ [SI] with a mean of $127 \cdot 10^{-6}$ [SI] and a standard deviation of $91 \cdot 10^{-6}$ [SI]. For specimens with $K_m > 10^{-3}$ [SI], the magnetic hysteresis loops and parameters (M_r/M_s and H_{cr}/H_c) indicate that titanomagnetite grains display various grain sizes ranging from pseudo-single domain (PSD) to multidomain (MD) (Fig. 6). Specimens with $K_m < 10^{-3}$ [SI], exhibit a broader scatter of hysteresis parameters mostly typical of PSD grains, although minor contributions from other ferromagnetic s.l. phases such as hematite or pyrrhotite cannot be excluded. The two groups overlap. FORC analysis confirms the hysteresis results and shows that coercivities have unimodal distributions. The PSD hysteresis values shown by specimen PU83A11 indicate only a minor contribution from interacting grains and therefore do not result from mixture between single-domain (SD) and multidomain grains. The ratio of high-field magnetic susceptibility to low-field magnetic susceptibility provides an approximation for the percentage of paramagnetic susceptibility. The percentage of paramagnetic susceptibility ranges widely with a median at 4% (Supplementary data 1).

4.3. Low-field magnetic susceptibility

The bulk magnetic susceptibility (K_m) of 1947 cubes and 120 stations ranges widely from $12 \cdot 10^{-6}$ [SI] to $31{,}600 \cdot 10^{-6}$ [SI], with an average of $4655 \cdot 10^{-6}$ [SI] (Figs. 7 and 8A and B; Supplementary data 2). K_m, both at the cube level and at the station level, shows a broadly bimodal pattern hence defining two subgroups: (A) with $K_m < 1000 \cdot 10^{-6}$ [SI]; (B) with $K_m \geq 1000 \cdot 10^{-6}$ [SI] (Figs. 7 and 8A). The theoretical maximum paramagnetic magnetic susceptibility (K_{para}) is calculated using Syono's (1960) method, which deduces the total Bohr magnetons from percentages of Fe^{2+}, Fe^{3+} and Mn^{2+} cations. Using whole-rock geochemical data from Beakhouse et al. (2011), and following the approach of Aydin et al. (2007), we obtain $K_{para} = 130 \cdot 10^{-6}$ [SI]. Any specimen with a magnetic susceptibility higher than this value must host ferromagnetic phases (Fig. 8A and B).

4.4. Anisotropy of magnetic susceptibility

The corrected degree of anisotropy (P') ranges widely from 1.008 to 1.827, although most values fall below 1.300 (Fig. 8A and C; Supplementary data 2). P' displays a slight positive correlation with K_m in subgroups A and B. The maximum value of paramagnetic anisotropy P_{para} is defined by the most abundant paramagnetic mineral which, in general, is biotite with a $P_{biot} = 1.30$ (Tarling and Hrouda, 1993). Any specimen with a degree of magnetic anisotropy higher than this value must have an AMS controlled by ferromagnetic phases (Fig. 8A and C). Few specimens ($\approx$4%) fall into the paramagnetic range defined by $K_{para} < 130 \cdot 10^{-6}$ [SI] and $P_{para} < 1.30$ (Fig. 8A). The shape parameter, T, covers the entire spectrum from +1 to −1 with no clear dominance of either prolate or oblate fabric (Fig. 8B). The two subgroups A and B faintly appear on this plot. The variation of the three AMS scalar parameters K_m, T and P' can also be visualized in 3-D in an animation produced with the 3D Data Visualizer Pro 1.0.8. software (Supplementary data 3).

The macroscopic foliation of 10 randomly selected specimens was measured with a Brunton compass on three mutually perpendicular faces of the oriented samples used for preparation of the AMS cubes. The macroscopic foliation plots less than 20° away from the magnetic foliation which confirms that the AMS constitutes a valid proxy for macroscopic foliation (Fig. 9).

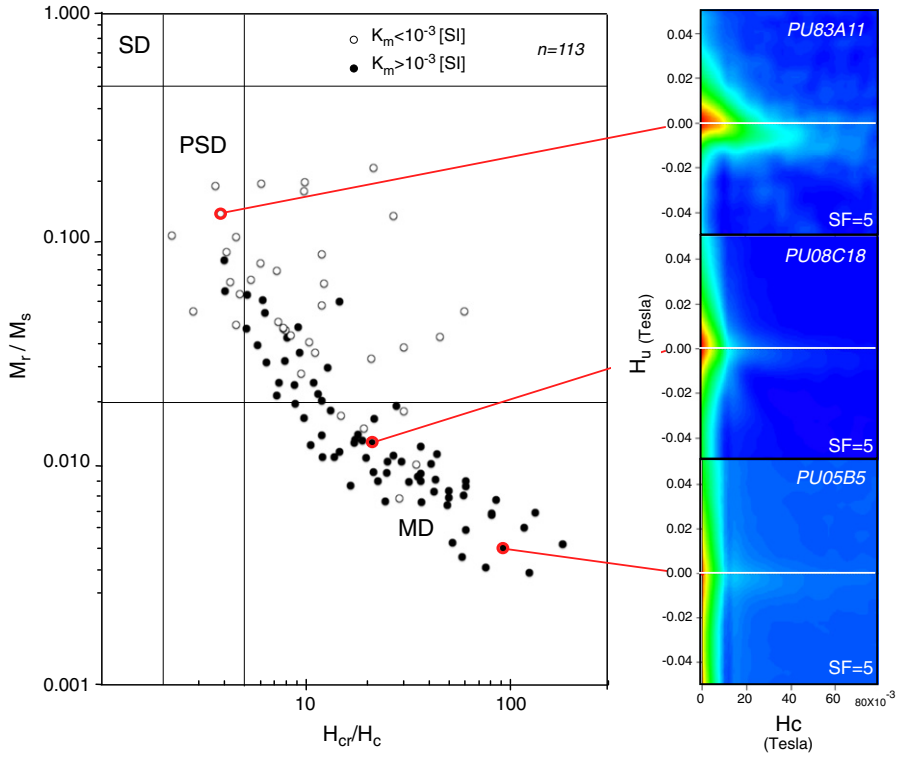

Fig. 6. Magnetic hysteresis ratios plotted in a Dunlop (2002) plot. M_r/M_s versus H_{cr}/H_c from 113 samples (one from each station). This plot indicates a mixture of multidomain (MD) and pseudo-single domain (PSD) grain sizes. The First Order Reversal Curve (FORC) diagrams are plotted using FORCinel (Harrison and Feinberg, 2008). See text for details.

Three types of AMS fabric can be distinguished based on their symmetry (Fig. 10, Supplementary data 2 and 4): (A) dominantly oblate AMS fabrics at the cube scale define planar symmetry at the station scale; the symmetry is illustrated by a relatively wide girdle of K_1 lineations and tightly clustered K_3 foliations (Fig. 10A); (B) dominantly prolate AMS fabrics at the cube scale define linear symmetry at the station scale; the symmetry is shown by a cluster of K_1 lineations and a relatively wide girdle of K_3 foliations (Fig. 10B); and (C) other AMS fabrics display relatively clustered K_1 and K_3 axes that define a plano-linear symmetry (Fig. 10C). Seventy seven percent of stations display a plano-linear symmetry, while planar and linear symmetries respectively account for 17% and 7% of stations.

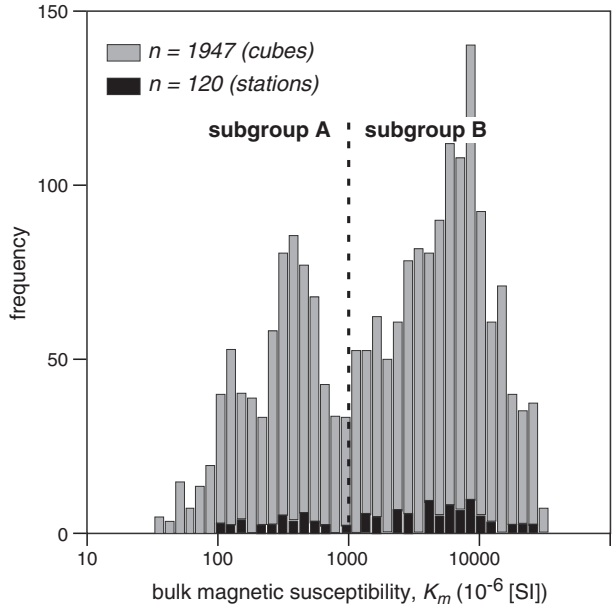

Fig. 7. Histogram of bulk magnetic susceptibility, K_m. The bimodal distribution defines two subgroups, A and B, above and below 10^{-3} [SI] respectively.

Most stations near the HSZ show a plano-linear symmetry, with K_1 lineations parallel to the HSZ contact (Fig. 11). This fabric defines structural domain B. Away from the contact with the greenstone belt, lineations and foliations are generally oriented in different attitudes in a less organized fashion and generally show a planar symmetry fabric. Magnetic lineations consistently trend SW–NE and are relatively shallow within a 3 to 5 km-wide domain referred to as domain C (Fig. 11). Magnetic lineations broadly trend NS along the shoreline of Lake Superior (Domain A in Fig. 11). The degree of magnetic anisotropy (P') in all three structural domains remains similar to the rest of the complex. Conversely, microstructures in these domains are highly equilibrated and similar to the main part of the complex. These microstructures support the absence of low- to medium temperature deformation and to the contrary indicate magmatic to high-temperature plastic deformation.

5. Interpretation and discussion

The relatively large grain size of titanomagnetite grains (5–200 μm, Fig. 3B) along with their euhedral shape supports a primary magmatic origin. The thermomagnetic data in Fig. 5 establishes the presence of a strongly ferromagnetic phase with a Curie temperature of 551 °C. Further, the distinct Hopkinson peak characterizes populations of multidomain titanomagnetite (King and Ranganai, 2001). Also, the magnetic hysteresis data in Fig. 6 supports that mixtures of pseudo-single domain and multidomain titanomagnetite form the main ferromagnetic source. The contributions of ferromagnetic and paramagnetic phases to magnetic susceptibility, deduced from magnetic hysteresis data (Supplementary data 1) vary greatly between specimens but have medians at about 96% and 4% respectively. The paramagnetic contribution, evaluated through the method of Syono, yields a maximum value of $K_{para} \approx 130 \cdot 10^{-6}$ [SI]. This value also corresponds to 4%

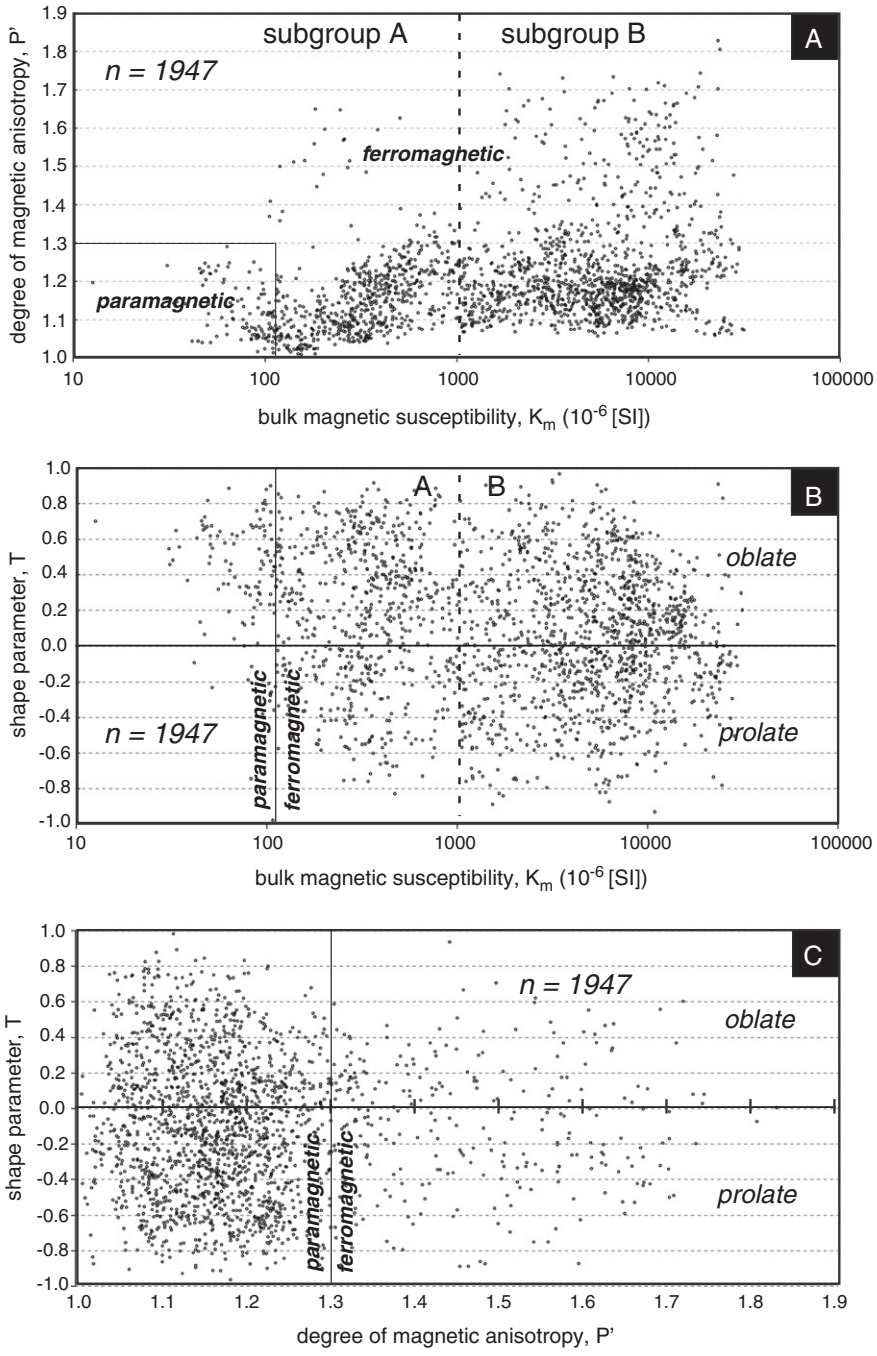

Fig. 8. Bulk anisotropy of magnetic susceptibility for all PIC specimens. A — The degree of magnetic anisotropy, P', versus bulk magnetic susceptibility, K_m. B — Shape parameter, T, versus bulk magnetic susceptibility, K_m, showing comparable numbers of prolate and oblate specimens. C — Shape parameter, T, versus degree of magnetic anisotropy, P', illustrating that T is independent from P'.

of the median low-field magnetic susceptibility of $3180 \cdot 10^{-6}$ [SI] (Supplementary data 2). Out of 1947 specimens, 150 (7.7%) have a magnetic susceptibility less than $130 \cdot 10^{-6}$ [SI] and therefore could potentially be paramagnetic only. In summary, all magnetic measurements and calculations point to multidomain titanomagnetite as the main source of low-field magnetic susceptibility.

Since titanomagnetite grains dominate the magnetic susceptibility and form elongate grains parallel to mafic silicates (Fig. 3B), they should collectively form a magnetostatic anisotropy and control the AMS. Considering that the intrinsic magnetic anisotropies of biotite and amphibole are $P_{biot} = 1.35$ and $P_{amph} = 1.65$ (Tarling and Hrouda, 1993), and that a volume $x \approx 0.15\%$ at most of these minerals would contribute to lattice preferred orientation (LPO), the anisotropic component of magnetic susceptibility due to these silicates (K_{para}) would range approximately between $(x \cdot (P_{biot} - 1))$. $P_{paraMax}$ in biotite-dominated gneisses and $(x \cdot (P_{amph} - 1))$. $P_{paraMax}$, in amphibole-dominated rocks, i.e., a modest directional variation of magnetic susceptibility (7 to $13 \cdot 10^{-6}$ [SI]). Therefore, even if the PIC rocks had preserved a strong silicate lattice-preferred orientation (LPO) of paramagnetic silicates through recrystallization, the modest contribution of paramagnetic minerals to AMS would be insignificant in comparison to the large contribution of titanomagnetite.

The Pukaskwa quartzo-feldspathic gneisses exhibit microstructures similar to those formed during high-temperature plastic flow

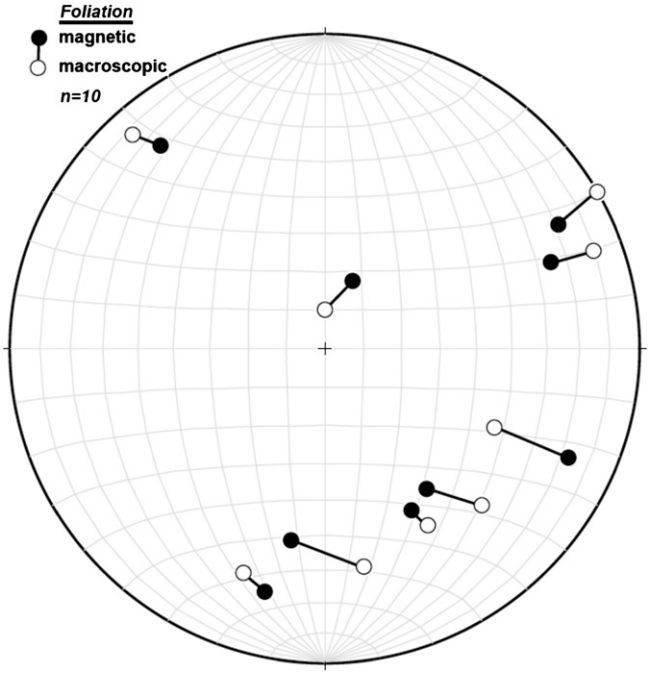

Fig. 9. Lower hemisphere, equal area stereonets comparing macroscopic foliation measured on three mutually perpendicular faces of 10 oriented samples with the magnetic foliation (plane to K_3). The excellent correspondence (<20° departure) validates the use of AMS as a proxy for macroscopic structures.

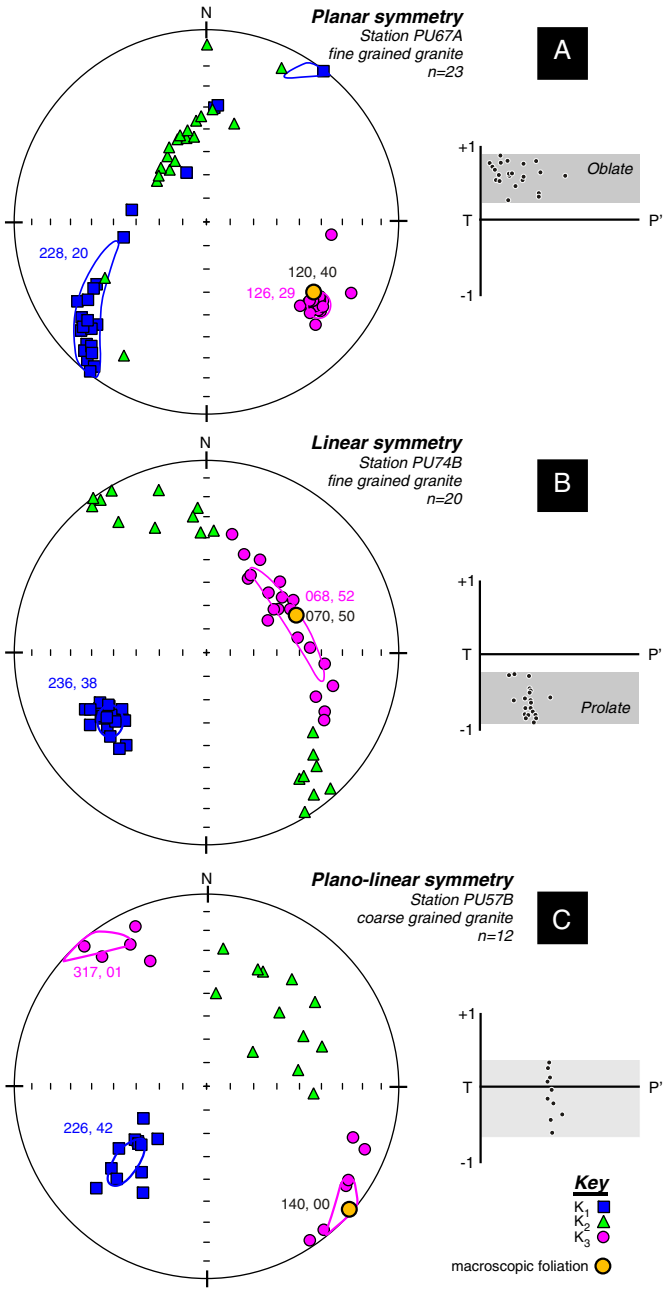

Fig. 10. Stereonets of magnetic fabric symmetries (planar, linear and plano-linear) at the station scale that arise from the distribution of AMS fabrics (oblate, prolate and general) at the cube scale. A — Dominantly oblate shape parameter showing girdled K_1 axes and clustered K_3 axes. B — Dominantly prolate shape parameter showing strong clustered K_1 axes and girdled K_3 axes. C — Plano-linear specimens show a maxima for K_1 and K_3 axes.

in a magma or in a metamorphic rock (e.g., Ferré and Améglio, 2000; Ferré et al., 2003; Gébelin et al., 2006; Kruckenberg et al., 2010, 2011). In general, plutonic rocks emplaced near shear zones display microstructures indicative of high strain-rate and high-temperature (e.g., Nouar et al., 2011). In contrast, most PIC rocks exhibit highly equilibrated microstructures. Also, previous studies on similar rocks have shown that multidomain titanomagnetite grains, deformed in similar high-temperature and low strain rate conditions, develop a shape-preferred orientation (SPO) due to dislocation creep, which in turn causes the magnetostatic anisotropy of titanomagnetite (Charles et al., 2009; Ferré et al., 2003, 2004; Kruckenberg et al., 2010, 2011; Schulmann et al., 2009; Till et al., 2012). The same studies also showed that magnetite-controlled AMS fabrics display general AMS ellipsoids, such as those shown in Fig. 10A and B, instead of planar and linear ellipsoids that more commonly originate from magnetocrystalline anisotropy. Also, the increase of P' with increasing K_m observed mostly for subgroup B is typical of AMS carried by magnetite (e.g., Bouchez, 1997). The variations in degree of magnetic anisotropy (P') or shape factor (T) across the PIC do not display a consistent spatial pattern. The lack of significant post-emplacement deformation in the PIC (Beakhouse et al., 2011; Lin, 2001) suggests that the AMS represents a fabric acquired during high-temperature plastic or magmatic deformation in the Archean.

In this study, the AMS provides new structural information on finite strain in the PIC that, away from the HSZ, lacks macroscopic strain markers. The AMS principal axes, obtained from a large number of specimens (about 20), are statistically significant as illustrated by AMS ellipses (Fig. 10 and Supplementary data 4). Previous studies show that in high-grade gneisses, the AMS K_1 axis parallels the mineral stretching lineation (Charles et al., 2009; Ferré et al., 2003, 2004; Kruckenberg et al., 2010, 2011; Schulmann et al., 2009) and therefore provides precious kinematic information on high-temperature flow. In general, in the PIC, K_1 axes plunge shallowly to moderately (Fig. 10A), including in the vicinity of the HSZ.

The AMS of granitic and metamorphic rocks always records finite strain, including the last increment of deformation. In the case of the PIC, AMS fabrics are very consistent at the scale of several square kilometers. The lack of medium or low-temperature plastic deformation in these rocks indicates that these AMS fabrics actually represent late Archean (D_2) high-temperature plastic flow. The dip-slip stretching lineations observed in some metasedimentary rocks within the HSZ (Fig. 2D) may reflect early kinematics (D_1) or syn D2 transpressional deformation. The corridors of homogeneous magnetic fabric orientation (e.g., domain C in Figs. 11 and 12) may record ductile strain localization, a structural feature documented in other anatectic domes in Brazil (Archanjo et al., 2013).

The structural and AMS fabric data indicate a systematic vergence of foliations dipping 40–45° to the North (Fig. 10). The dip angle of

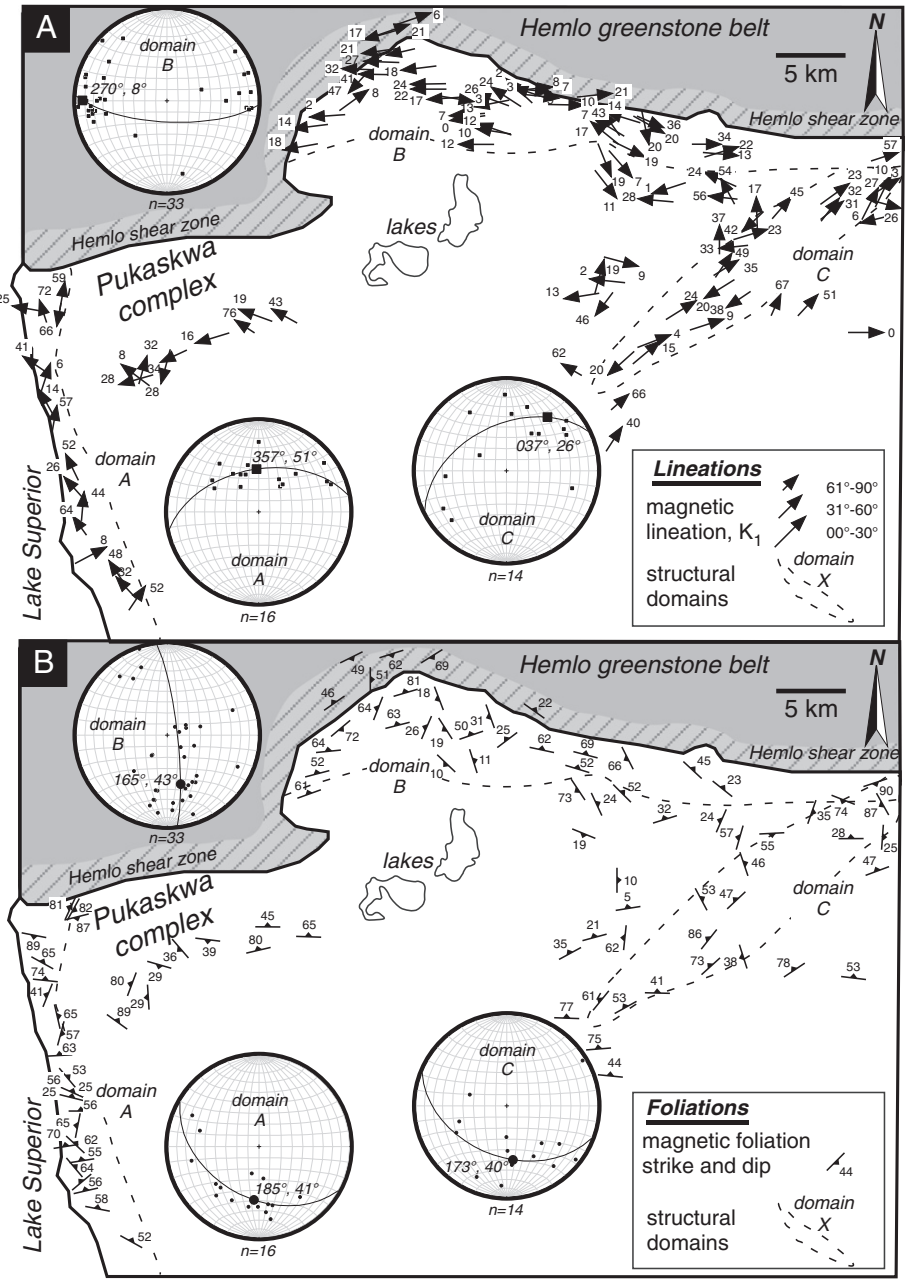

Fig. 11. Magnetic fabrics in the PIC complex. Lineation trends and plunges are plotted with respect to station localities. Arrow size defines a range of plunge angles (short arrows, 61°–90°; medium arrows, 31°–60°; long arrows, 0°–30°).

foliation across the entire northern half of the Pukaskwa intrusive complex does not become shallower toward the center of the region referred to as Pukaskwa batholith by Lin and Beakhouse (2013). We also note that domain B displays significantly less steep foliations than in their diapirism–sagduction model. We propose an alternative structural interpretation in which the Hemlo shear zone, and domains B and C of the Pukaskwa intrusive complex share similar structural vergence to the SSE (Fig. 12). This model is characterized by early thrust tectonics with dip-slip lineations (domain A) followed by moderate strike-slip strain localization within the Pukaskwa intrusive complex (domain C) and intense strike-slip strain localization along major lithological contacts, along the Hemlo greenstone belt (domain B). Our model appears to be consistent with sinistral transpressive tectonics documented by Lin (2001) and Beakhouse and Davis (2005).

Archean migmatitic domains generally appear structurally complex (e.g., Hopgood, 1998) but here we show that these domains hold an internal fabric organization that can be unraveled by the use of magnetic methods.

6. Conclusions

AMS investigation allows a better understanding of the Pukaskwa emplacement. Three main domains characterize the northern margin of the PIC: Domain B, at the contact between the greenstone belt and the PIC, shows near horizontal magnetic lineations parallel to the Hemlo shear zone; Domain C, to the east-southeast of the study area, displays shallow magnetic lineations consistently trending SW–NE; and finally Domain A, defined along the shoreline of Lake Superior, indicates near consistent NS trending magnetic lineations. There is a general tendency for magnetic foliations to dip to the north. Yet, these domains are not characterized by either stronger magnetic fabrics or important solid-state deformation, to the contrary, all of them

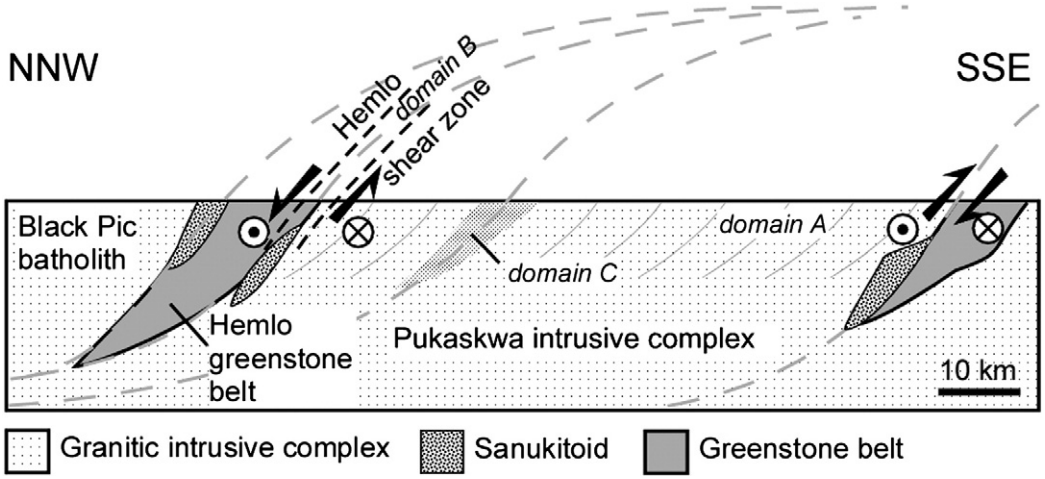

Fig. 12. Schematic tectonic model for the Hemlo shear zone and Pukaskwa intrusive complex. Foliations in the Pukaskwa intrusive complex generally dip NNW with dip-slip lineations, except along domain C where lineations display a strike-slip attitude.

exhibit fabrics acquired at high temperature. Our AMS data support the idea that the Pukaskwa emplacement occurred by rapid successive and small heterogeneous magma increments. The new dataset does not support a diapiric emplacement as suggested by Lin and Beakhouse (2013). Rather our AMS data indicate that the PIC was emplaced within a sinistral transpressive setting (Fig. 12) as recorded by mylonitic Archean metasedimentary and mafic metavolcanic rocks of the greenstone belt.

Supplementary data to this article can be found online at http://dx.doi.org/10.1016/j.tecto.2013.06.022.

Acknowledgments

We gratefully acknowledge the logistical support from various mining companies. This study was funded by a grant from the Natural Sciences and Engineering Research Council of Canada (NSERC) to S. Lin. Sarah A. Friedman provided assistance in the high-field magnetic measurements. The AMS data and ellipses of confidence were plotted using Anisoft 4.2 (Chadima and Jelínek, 2008). We thank R. Enjolvy for assistance during field work. The comments made by Carlos Archanjo and an anonymous reviewer greatly improved this research.

References

Archanjo, C.J., Viegas, L.G.F., Hollanda, M.H.B.M., Souza, L.C., Liu, D., 2013. Timing of the HT/LP transpression in the Neoproterozoic Serido Belt (Borborema Province, Brazil): Constraints from U/Pb (SHRIMP) geochronology and implications for the connections between NE Brazil and West Africa. Gondwana Research 23 (2), 701–714.

Aydin, A., Ferré, E.C., Aslan, Z., 2007. The magnetic susceptibility of granitic rocks as a proxy for geochemical composition: Example from the Sahuran granitoids, NE Turkey. Tectonophysics 441, 85–95.

Beakhouse, G.P., Davis, D.W., 2005. Evolution and tectonic significance of intermediate to felsic plutonism associated with the Hemlo greenstone belt, Superior Province, Canada. Precambrian Research 137, 61–92.

Beakhouse, G.P., Lin, S., Kamo, S.L., 2011. Magmatic and tectonic emplacement of the Pukaskwa batholith, Superior Province, Ontario, Canada. Canadian Journal of Earth Sciences 48 (2), 187–204.

Bouchez, J.L., 1997. Granite is never isotropic: An introduction to AMS studies of granitic rocks. In: Bouchez, J.L., Hutton, D.H.W., Stephens, W.E. (Eds.), Granite: from segregation of melt to emplacement fabrics, 8. Kluwer Publishing Co., Dordrecht, pp. 95–112.

Calvert, A.J., Ludden, J.N., 1999. Archean continental assembly in the southeastern Superior Province of Canada. Tectonics 18 (3), 412–429.

Card, K.D., 1990. A review of the Superior Province of the Canadian Shield, a product of Archean accretion. Precambrian Research 48, 99–156.

Chadima, M., Jelínek, V., 2008. Anisoft 4.2. — Anisotropy data browser. In: Hvožd'ara, M. (Ed.), Paleo, Rock and Environmental Magnetism, 11th Castle Meeting. Contribution to Geophysics and Geodesy, Special issue. Geophysical Institute of the Slovak Academy of Sciences, Bojnice Castle, Slovac Republic (41 pp.).

Chardon, D., Choukroune, P., Jayananda, M., 1996. Strain patterns, decollement and incipient sagducted greenstone terrains in the Archaean Dharwar craton (south India). Journal of Structural Geology 18 (8), 991–1004.

Chardon, D., Gapais, D., Cagnard, F., 2009. Flow of ultra-hot orogens: A view from the Precambrian, clues for the Phanerozoic. Tectonophysics 477 (3–4), 105–118.

Charles, N., Faure, M., Chen, Y., 2009. The Montagne Noire migmatitic dome emplacement (French Massif Central): New insights from petrofabric and AMS studies. Journal of Structural Geology 31 (11), 1423–1440.

Clark, D.A., 1997. Magnetic petrophysics and magnetic petrology: Aids to geological interpretation of magnetic surveys. Journal of Australian Geology and Geophysics 17 (2), 83–103.

Corfu, F., Muir, T.L., 1989a. The Hemlo–Heron Bay greenstone belt and Hemlo Au–Mo deposit, Superior Province, Ontario, Canada 1. Sequence of igneous activity determined by zircon U–Pb geochronology. Chemical Geology: Isotope Geoscience Section 79 (3), 183–200.

Corfu, F., Muir, T.L., 1989b. The Hemlo–Heron Bay greenstone belt and Hemlo Au–Mo deposit, Superior Province, Ontario, Canada 2. Timing of metamorphism, alteration and Au mineralization from titanite, rutile, and monazite U–Pb geochronology. Chemical Geology: Isotope Geoscience Section 79 (3), 201–223.

de Wit, M.J., 1998. On Archean granites, greenstones, cratons and tectonics: Does the evidence demand a verdict? Precambrian Research 91, 181–226.

Dixon, J.M., Summers, J.M., 1983. Patterns of total and incremental strain in subsiding troughs: Experimental centrifuged models of inter-diapir synclines. Canadian Journal of Earth Sciences 20 (12), 1843–1861.

Dunlop, D.J., 2002. Theory and application of the Day plo (Mrs/Ms versus Hcr/Hc) 2. Application to data for rocks, sediments, and soils. Journal of Geophysical Research: Solid Earth 107, 5–15. http://dx.doi.org/10.10129/2001JB000486.

Ferré, E.C., Améglio, L., 2000. Preserved magnetic fabrics vs. annealed microstructures in the syntectonic recrystallised George granite, South Africa. Journal of Structural Geology 22 (8), 1199–1219.

Ferré, E.C., Teyssier, C., Jackson, M.J., Thill, J.V., Rainey, E.S.G., 2003. Magnetic susceptibility anisotropy: A new petrofabric tool in migmatites. Journal of Geophysical Research 108 (B2). http://dx.doi.org/10.1029/2002JB001790.

Ferré, E.C., Martín-Hernández, F., Teyssier, C., Jackson, M.J., 2004. Paramagnetic and ferromagnetic anisotropy of magnetic susceptibility in migmatites: Measurements in high and low fields and kinematic implications. Geophysical Journal International 157 (3), 1119–1129.

Gébelin, A., Martelet, G., Chen, Y., Brunel, M., Faure, M., 2006. Structure of late Variscan Millevaches leucogranite massif in the French Massif Central: AMS and gravity modelling results. Journal of Structural Geology 28 (1), 148–169.

Hamilton, W.B., 1998. Archean magmatism and deformation were not products of plate tectonics. Precambrian Research 91, 143–179.

Hamilton, W.B., 2007. Earth's first two billion years —The era of internally mobile crust. Geological Society of America Memoirs 200, 233–296.

Harris, L.B., Godin, L., Yakymchuk, C., 2012. Regional shortening followed by channel flow induced collapse: A new mechanism for dome and keel geometries in Neoarchaean granite-greenstone terrains. Precambrian Research 212–213, 139–154.

Harrison, R.J., Feinberg, J.M., 2008. FORCinel: An improved algorithm for calculating first-order reversal curve distributions using locally weighted regression smoothing. Geochemistry, Geophysics, Geosystems 9 (Q05016). http://dx.doi.org/10.1029/2008GC001987.

Hasalova, P., et al., 2008. Origin of migmatites by deformation-enhanced melt infiltration of orthogneiss: A new model based on quantitative microstructural analysis. Journal of Metamorphic Geology 26 (1), 29–53.

Hopgood, A.M., 1998. Determination of Structural Successions in Migmatites and Gneisses. Kluwer Academic Pub., Dordrecht (346 pp.).
Jackson, S.L., 1998. Stratigraphy, structure and metamorphism, Part 1. Regional Setting of the Hemlo Gold Deposit: An Interim Progress Report, p. 5977.
King, J.G., Ranganai, R.T., 2001. Determination of magnetite grain-size using the Hopkinson effect — Examples from Botswana rocks. Botswana Journal of Earth Sciences 5, 35–38.
Kruckenberg, S.C., et al., 2010. Viscoplastic flow in migmatites deduced from fabric anisotropy: An example from the Naxos dome, Greece. Journal of Geophysical Research: Solid Earth 115 (B9), B09401.
Kruckenberg, S.C., Vanderhaeghe, O., Ferré, E.C., Teyssier, C., Whitney, D.L., 2011. Flow of partially molten crust and the internal dynamics of a migmatite dome, Naxos, Greece. Tectonics. http://dx.doi.org/10.1029/2010TC002751.
Lana, C., Tohver, E., Cawood, P., 2010. Quantifying rates of dome-and-keel formation in the Barberton granitoid-greenstone belt, South Africa. Precambrian Research 177 (1–2), 199–211.
Lin, S., 2001. Stratigraphic and structural setting of the Hemlo gold deposit, Ontario, Canada. Economic Geology 96 (3), 477–507.
Lin, S., 2005. Synchronous vertical and horizontal tectonism in the Neoarchean: Kinematic evidence from a synclinal keel in the northwestern Superior craton, Canada. Precambrian Research 139 (3–4), 181–194.
Lin, S., Beakhouse, G.P., 2013. Synchronous vertical and horizontal tectonism at late stages of Archean cratonization and genesis of Hemlo gold deposit, Superior craton, Ontario, Canada. Geology 41 (3), 359–362.
Lister, G.S., Davis, G.A., 1989. The origin of metamorphic core complexes and detachment faults formed during Tertiary continental extension in the northern Colorado River region, U.S.A. Journal of Structural Geology 11 (1–2), 65–94.
Martín-Hernández, F., Ferré, E.C., 2007. Separation of paramagnetic and ferrimagnetic anisotropies: A review. Journal of Geophysical Research: Solid Earth 112. http://dx.doi.org/10.1029/2006JB004340.
Nouar, O., Henry, B., Liégeois, J.P., Derder, M.E.M., Bayou, B., Bruguier, O., Ouabadi, A., Amenna, M., Hemmi, A., Ayache, M., 2011. Eburnean and Pan-African granitoids and the Raghane mega-shear zone evolution: Image analysis, U–Pb zircon age and AMS study in the Arokam Ténéré (Tuareg shield, Algeria). Journal of African Earth Sciences 60 (3), 133–152.
Percival, J.A., 1994. Archean high-grade metamorphism. In: Condie, K.C. (Ed.), Developments in Precambrian Geology, Chapter 9. Elsevier, pp. 357–410.
Percival, J.A., Stern, R.A., Skulski, T., 2001. Crustal growth through successive arc magmatism: Reconnaissance U–Pb SHRIMP data from the northeastern Superior Province, Canada. Precambrian Research 109 (3–4), 203–238.
Pokorny, J., Suza, P., Hrouda, F., 2004. Anisotropy of magnetic susceptibility of rocks measured in variable weak magnetic fields using the KLY-4S Kappabridge. Geological Society, London, Special Publications 238 (1), 69–76.
Polteau, S., Ferré, E.C., Planke, S., Neumann, E.R., Chevallier, L., 2008. How are saucer-shaped sills emplaced? Constraints from the Golden Valley Sill, South Africa. Journal of Geophysical Research: Solid Earth 113 (B12104). http://dx.doi.org/10.1029/2008JB005620.
Sandiford, M., Van Kranendonk, M.J., Bodorkos, S., 2004. Conductive incubation and the origin of dome-and-keel structure in Archean granite-greenstone terrains: A model based on the eastern Pilbara Craton, Western Australia. Tectonics 23. http://dx.doi.org/10.1029/2002TC001452.
Schulmann, K., Edel, J.B., Hasalova, P., Cosgrove, J., Jezek, J., Lexa, O., 2009. Influence of melt induced mechanical anisotropy on the magnetic fabrics and rheology of deforming migmatites, Central Vosges, France. Journal of Structural Geology 31 (10), 1223–1237.
Shackleton, R.M., 1995. Tectonic evolution of greenstone belts. Geological Society, London, Special Publications 95 (1), 53–65.
Snowden, P.A., Bickle, M.J., 1976. The Chinamora Batholith: Diapiric intrusion or interference fold? Journal of the Geological Society 132 (2), 131–137.
Syono, Y., 1960. Magnetic susceptibility of some rock forming silicate minerals such as amphiboles, biotites, cordierites and garnets. Journal of Geomagnetism and Geoelectricity 11, 85–93.
Tarling, D.H., Hrouda, F., 1993. The magnetic anisotropy of rocks. Chapman & Hall, London (217 pp.).
Till, J.L., Moskowitz, B.M., Jackson, M.J., 2012. High-temperature magnetic fabric development from plastically deformed magnetite in experimental shear zones. Geophysical Journal International 189 (1), 229–239.
Van Kranendonk, M.J., Hugh Smithies, R., Hickman, A.H., Wingate, M.T.D., Bodorkos, S., 2010. Evidence for Mesoarchean (3.2 Ga) rifting of the Pilbara Craton: The missing link in an early Precambrian Wilson cycle. Precambrian Research 177 (1–2), 145–161.
Williams, H.R., Stott, G.M., Heather, K., Muir, T.L., Sage, R.P., 1991. Wawa Subprovince. In: Thurston, P.C., Williams, H.R., Sutcliffe, R.H., Stott, G.M. (Eds.), Geology of Ontario. Ontario Geological Survey, pp. 485–539.